

OBSERVING AND FORECASTING VOG DISPERSION FROM KĪLAUEA VOLCANO, HAWAII

BY STEVEN BUSINGER, ROY HUFF, ANDRE PATTANTYUS, KEITH HORTON,
A. JEFF SUTTON, TAMAR ELIAS, AND TIZIANA CHERUBINI

A program to measure and forecast the dispersion of hazardous volcanic emissions from the Kīlauea volcano in Hawaii is described.

In 2014, Kīlauea volcano on the island of Hawaii entered its 32nd year of nearly continuous eruption. The current activity began in January 1983 and the first 4 years of the eruption included sensational episodes of lava fountains. During the high-fountaining events, sulfur dioxide (SO_2) emissions from Kīlauea's east rift zone ranged from 5,000 to 30,000 tonnes of SO_2 per day (Casadevall et al. 1987). Since 1986, east rift SO_2 emissions have ranged from <50 tonnes during the periods of eruptive pause to over 10,000 tonnes per day during periods of enhanced activity (Elias et al. 1998; Elias and Sutton 2002, 2007, 2012). Sulfur dioxide and other gases released from Kīlauea's emission sources

FIG. 1. Map showing the island of Hawaii with the relative locations of the volcanic vents, Volcano village, the cities of Hilo and Kailua-Kona, and the SO_2 and SO_4 observation sites.

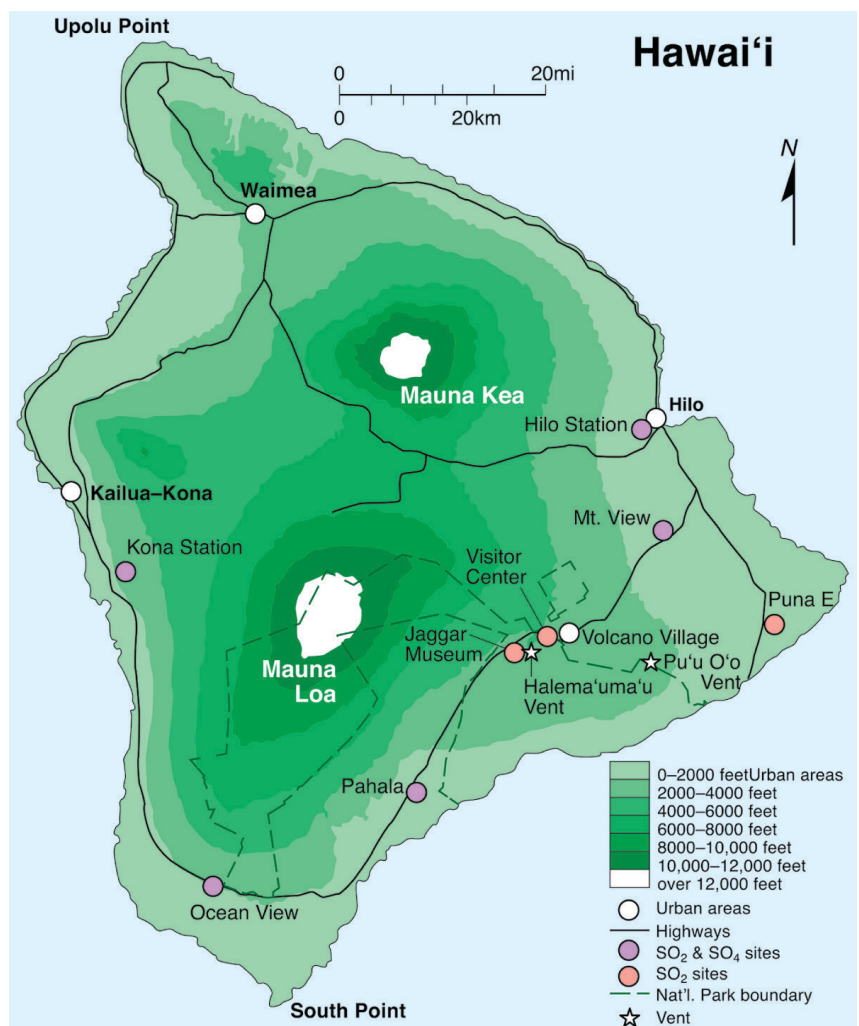




FIG. 2. Gas and particle plume continuously emitted from vent within Halema'uma'u Crater.

react with oxides and atmospheric moisture to produce volcanic smog, known locally as “vog” (Sutton et al. 2001).

Emissions from Pu'u 'Ō'ō, the largest vent along the east rift zone, affect the southeastern portion of Hawai'i Volcanoes National Park every trade wind day (Fig. 1). An air quality monitoring station located at the National Park Visitor Center recorded over 70 days between 1986 and 1997 when the Environmental Protection Agency's primary (24 h) health standard of 0.14 ppm was exceeded (Elias 1992; Sutton and Elias 1993, 1997). More recently, summit SO_2 emissions reached record high levels when a new vent opened within the Halema'uma'u Crater in March 2008 (Fig. 2), with the first explosive eruption at Kilauea's summit since 1924 (Wilson et al. 2008). Under weather patterns that produce southerly winds, emissions

from Halema'uma'u are advected through Kilauea's summit area within the park, which is visited by ~3 million people each year. From there the vog frequently passes over and through Volcano village, located ~4 km northeast of the Halema'uma'u Crater. In recent years, Kilauea has been releasing, on average, an order of magnitude more SO_2 than the single dirtiest power plant on the U.S. mainland.¹

The result of continued enhanced emissions has had significant environmental impacts, including effects on agriculture, infrastructure,

and human populations (Elias et al. 2009; Longo et al. 2010). With the onset of the summit activity in 2008, episodes of high ambient SO_2 along with particle matter characterized by a mean diameter of less than $2.5 \mu\text{m}$ ($\text{PM}_{2.5}$) in both windward and leeward communities have increased dramatically. For example, between April 2008 and November 2009, Pahala, the closest downwind community, exceeded the Environmental Protection Agency (EPA) SO_2 or $\text{PM}_{2.5}$ 24-h primary health standard (0.14 ppm and $35 \mu\text{g m}^{-3}$, respectively) 8% of the time, and the annual average SO_2 concentration was more than twice the EPA standard (Elias et al. 2009). In 2013, the American Lung Association gave Hawaii County a failing grade in its “State of the Air” report with respect to the $\text{PM}_{2.5}$ pollution.

It should be noted that observed $\text{PM}_{2.5}$ pollution concentration, in addition to vog, also includes fine dust, smoke, and pollution from vehicles and utilities. We use $\text{PM}_{2.5}$ as a proxy for vog sulfate aerosol concentrations. By noting the $\text{PM}_{2.5}$ concentrations when vog is absent by virtue of the wind direction, we can control for the bias introduced by the background contribution from aerosol sources other than vog.

Data collected by Mather et al. (2012) suggest that sulfate aerosol represents the primary $\text{PM}_{2.5}$ component in the emission by orders of magnitude and represents ~1% by mass of SO_2 concentrations measured in the plume simultaneously. Kilauea's SO_2 emissions go through several chemical

AFFILIATIONS: BUSINGER, HUFF, PATTANTYUS, HORTON, AND CHERUBINI—University of Hawai'i at Mānoa, Honolulu, Hawaii; SUTTON AND ELIAS—Hawaiian Volcano Observatory, USGS, Hawaii National Park, Hawaii

CORRESPONDING AUTHOR: Steven Businger, Department of Atmospheric Sciences, University of Hawai'i at Mānoa, 2525 Correa Rd., Honolulu, HI 96822
E-mail: businger@hawaii.edu

The abstract for this article can be found in this issue, following the table of contents.

DOI:10.1175/BAMS-D-14-00150.1

In final form 8 May 2015
©2015 American Meteorological Society

¹ For more information see www.epa.gov/airmarkets/progress/datatrends/summary.html.

transformations after they enter the atmospheric boundary layer (Morrow 1991). McGonigle et al. (2004) found that SO₂ fluxes showed negligible variation with plume age or diurnal variations in temperature, relative humidity, and insolation, providing confirmation that remote SO₂ flux measurements (typically of ~500–2000-s-old plumes) are reliable proxies for source emissions for ash-free tropospheric plumes not emitted into cloud or fog. However, lidar and sun photometer measurements taken of the Kilauea plume show that the half-life of SO₂ in converting to aerosol is approximately 6 h (Porter et al. 2002). A more recent study based on analysis of SO₂ densities derived from satellite measurements suggests that the effective SO₂ lifetime in the Kilauea environment is on the order of 1–2 days (Beirle et al. 2013). The resulting sulfate aerosol is hygroscopic and remains in solution at ambient relative humidity. The hygroscopic nature allows the aerosol to expand up to 3 times its original volume (Porter and Clarke 1997). At 70% relative humidity, typical of Hawaii trade wind conditions, sulfate aerosol is ~30% sulfuric acid and ~70% water (Palmer and Williams 1975).

In addition to modeling volcanic emissions, there have been recent efforts to simulate the dispersion and evolution of anthropogenic SO₂ using more comprehensive chemical transport models (Schiferl et al. 2014; Fast et al. 2014; Forkel et al. 2014; Im et al. 2015). Schiferl et al. (2014) modeled SO₂ as part of California Research at the Nexus of Air Quality and Climate Change (CalNex) and their results using the Goddard Earth Observing System chemical transport model (GEOS-Chem) show underestimates of SO₂ in the Central Valley of California and an overestimate of near-surface sulfate, suggesting the oxidation of SO₂ to sulfate is too robust in the model, while sulfate is underpredicted near Los Angeles. Fast et al. (2014) use the Weather Research and Forecasting Model with Chemistry (WRF-Chem) to model regional aerosol variability over California and to find that diurnally averaged simulated sulfate was underforecasted in Southern California but better represented in Northern California.

The small particle sizes that characterize the sulfuric acid aerosol have very slow settling velocities, and thus the aerosol accumulates in the boundary layer under light wind conditions. It is these particulates that most strongly impact visibility. During episodes of increased sulfate production and atmospheric stagnation, the vog aerosol concentration may become high enough, particularly near the trade wind inversion, to create a significant visibility hazard for general aviation (R. Ballard 2012, personal communication) (Fig. 3).

The small size of the sulfate particulates found in Kilauea's emissions allows them to be drawn deeply into the lung, where they can be especially irritating to sensitive individuals. In addition to the submicron sulfate particles, SO₂ gas present in vog dissolves in and acidifies moist tissues of the respiratory tract, resulting in another source of irritation. Beyond lung irritation, the presence of vog has also been shown to exacerbate symptoms of asthma, sinusitis, and respiratory disease (Kleinman 1995; Ruben et al. 1995; Mannino et al. 1995; Worth 1995; Tam et al. 2007; Longo et al. 2010; Longo 2013).

Vog dispersion is primarily a function of synoptic and local wind patterns, as well as atmospheric stability. The majority of the vog pollutants are trapped within the subtropical boundary layer in the vicinity of Hawaii by a strong prevailing inversion (Fig. 3b). The inversion is the result of a persistent North Pacific high pressure system centered just northeast of the Hawaiian Islands, which is also responsible for northeast trade winds that characterize Hawaii's weather. The prevailing trade winds advect the vog pollutants from their source toward the southwest. Island blocking of the trade wind flow produces a clockwise

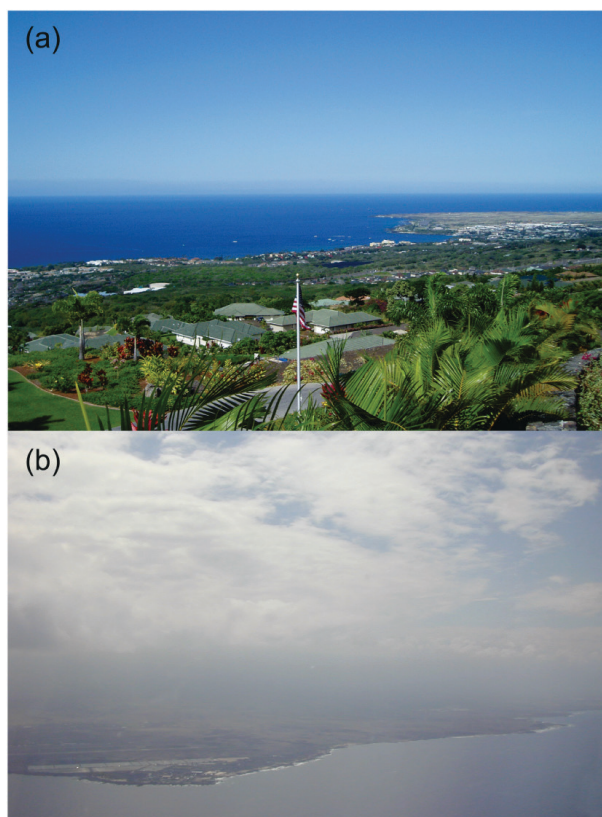


FIG. 3. (a) Kona coast on a clear day. (b) Vog layer trapped beneath trade wind inversion along the Kona coast.

eddy to the west of South Point (Fig. 1), which advects the vog first northward and then eastward toward the leeward coast (Leopold 1949; Schroeder 1981; Kodama and Businger 1998). Vog is carried onshore during the afternoon hours, when solar heating of the land surface along with light winds on the leeward coast result in a strong localized sea-breeze circulation (Schroeder 1981; Kodama and Businger 1998). Therefore, vog concentrations are enhanced along the Kona coast of the island of Hawaii during prevailing trade wind conditions. Weak inversions, strong trade winds, and persistent southerly winds (associated with fronts, shear lines, or kona lows) all act to reduce vog concentrations along the Kona coast.

Previous attempts to model volcanic emissions have been done for Mt. Etna in Italy (Barsotti et al. 2008; Favelli et al. 2004) and Eyjafjallajökull volcano in Iceland (Colette et al. 2011; Heinhold et al. 2012; Matthias et al. 2012; Perrone et al. 2012). Favelli et al. (2004) found that mesoscale model output provides better wind data than nearby surface stations to predict the transport of sulfur dioxide emissions. Barsotti et al. (2008) simulated ash dispersal from Mt. Etna during a 2001 eruption and found good agreement between modeled dispersion of small particles ($<30 \mu\text{m}$) and satellite images. More recently, the eruption of Eyjafjallajökull in 2010 resulted in a number of modeling studies for volcanic gas, ash, and particulates. Perrone et al. (2012) found that the Flexible Particle

dispersion model (FLEXPART) accurately simulated the arrival of volcanic ash, including simulated size distributions and vertical and temporal variability, but tended to overestimate total columnar ash concentrations over southern Italy by an order of magnitude. Colette et al. (2011) used the CHIMERE regional chemistry and transport model to forecast PM_{10} levels in France. They found that the arrival of the volcanic plume is handled well by the model when compared with observations; the model footprint of the plume matches surface observations of PM_{10} . The plume's evolution over the first 48 h is well represented by the model; however, the model tends to underestimate surface concentrations. Similar studies by Matthias et al. (2012) and Heinhold et al. (2012) highlight the limitations of quantitative forecasts of ash concentrations by uncertainties in emission parameters (mass, emission rate, size distribution, injection height, etc.).

The goal of the Vog Measurement and Prediction (VMAP) project is to mitigate the hazards associated with the emissions from Kilauea volcano to the Hawaiian community through improved monitoring of volcanic emissions and the development and rapid dissemination of an accurate numerical forecast of vog dispersion to the public. The stakeholders that are collaborating on this effort include the Hawaii State Civil Defense, the Hawaii State Department of Health, the U.S. Geological Survey (USGS), the Hawaiian Volcano Observatory (HVO), the National Oceanic and Atmospheric Administration (NOAA), and the National Park Service.

MONITORING SULFUR DIOXIDE EMISSIONS.

The SO_2 emission rate is a critical initial condition for an accurate vog dispersion model forecast. Emission rate data for input to the vog dispersion model in this research is a weekly average of the data collected along Crater Rim Drive and Chain of Craters Road, located within Hawai'i Volcanoes National Park (Fig. 4), by a vehicle-mounted UV spectrometer system called FLYSPEC (Horton et al. 2006, 2003; Elias et al. 2006;

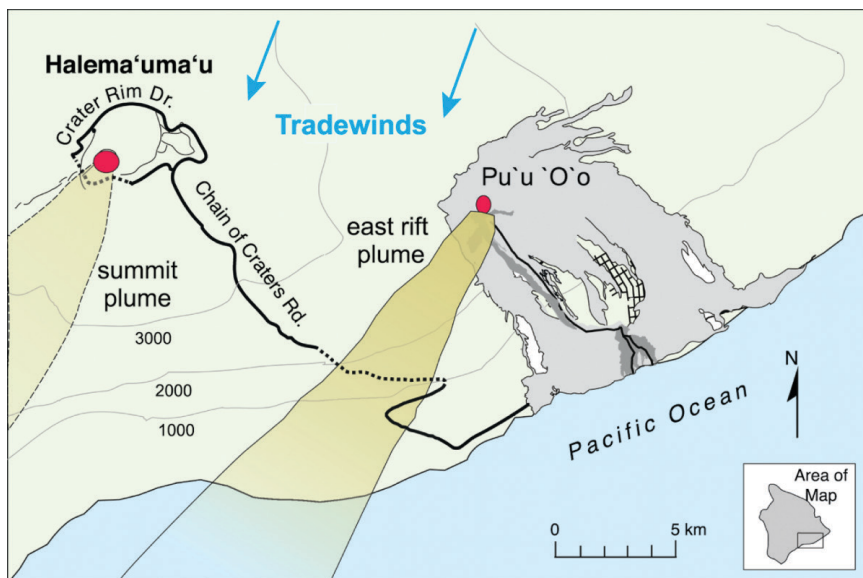


FIG. 4. Vehicle-based SO_2 measurements made downwind of the Pu'u 'O'o and Halema'uma'u vents on Chain of Craters Road and Crater Rim Drive. Location of vents (red circles) and plumes (yellow shading) are given for prevailing trade wind conditions. Gray shading represents the extent of recent lava flows in the east rift zone.

Elias and Sutton 2012). Multiple transects below the emission plume allow FLYSPEC to observe the extinction of UV light due to sulfur dioxide gas. This is accomplished by the differential optical absorption spectroscopy (DOAS) method (Perner and Platt 1980; Platt 1994). GPS data and spectral concentrations are used to determine integrated column amounts of SO_2 . This value is multiplied by the wind speed to derive SO_2 fluxes. Emissions data have been collected nominally 2–3 times per week since 1979, making it one of the best-documented volcanic SO_2 emission sources on the planet (Sutton et al. 2001). Accurate vehicle-based emission rate measurements at Kilauea require specific wind conditions near the vents. At the Thomas A. Jaggar Museum, 10-m winds are continuously observed and are also available from 1-km-resolution wind forecasts available from the Mauna Kea Weather Center (MKWC). Sulfate aerosol emissions at the vent are relatively small compared to the downwind conversion from SO_2 to sulfate aerosol. The sulfate aerosol emission is not measured operationally at the vent, and thus it has not been included in the Vog model initial condition to date. Measurements by Mather et al. (2012) indicate that the primary sulfate is about 1% of the SO_2 emission.

Modifications were made to the design of the commercially available FLYSPEC instrument, and an array of 10 of these stand-alone systems was constructed with Wi-Fi communications to transmit the collected data back to HVO in real time (Fig. 5) (Horton et al. 2012). Data from the array show the variation of the SO_2 plume cross section with 1-s time resolution, allowing comparisons with high-time-resolution geophysical parameters, such as seismicity (Fig. 6a). Correlations between SO_2 flux and seismicity have been demonstrated previously at Kilauea (Nadeau et al. 2011; Elias et al. 2012), and are strongly supported by the continuous record from the FLYSPEC array measurements (Fig. 6b). Similar correlations have been previously documented for the Villarrica volcano in Chile (Palma et al. 2008).

Since the opening of the new vent within Halema'uma'u Crater, the plume pathlength concentrations have been high enough to affect the accuracy of the SO_2 retrievals. The spectral retrievals are conducted in the conventional 305–315-nm range, where SO_2 absorption is strong. Because not all of the source light passes straight through the optically thick plume to the sensor, the retrievals have underestimated the SO_2 emission rates by anywhere from 20% to 90% (Elias et al. 2012; Kern et al. 2012). A dual-fit-window approach to data processing has been developed in which a second spectral window at longer wavelengths,

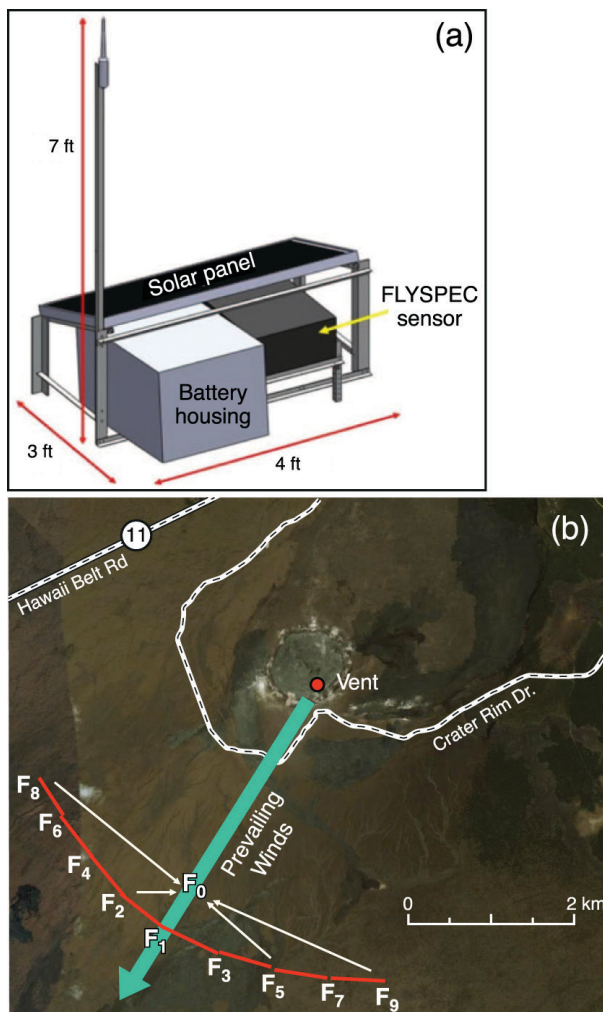


FIG. 5. (a) Schematic diagram of FLYSPEC instrument configuration with 160-W solar panel. FLYSPEC sensor, electronics, and computer are in the black box under the aluminum housing that supports the solar panel. Gray box contains the deep cycle battery and charge controller. (b) Aerial view of approximate sensor locations for the SO_2 monitoring array. Sensor array is located approximately 2.7 km from source vent at Halema'uma'u.

where SO_2 is less absorbing (319–330 nm), is utilized. For Kilauea's current summit eruption plume, the dual-window approach shows excellent promise for providing more accurate retrievals than the short single-window method, and is doing so across a wide range of pathlength concentrations of SO_2 within the plume, including those greater than $2,000 \text{ ppm} \times \text{m}$ [$100 \text{ ppm} \times \text{m} = 10 \text{ Dobson units (DU)}$]. As of January 2014, the more accurate array data are being used in the initial conditions for the Vog model.

TOWARD DEVELOPMENT OF AN OPERATIONAL DISPERSION MODEL. An automated

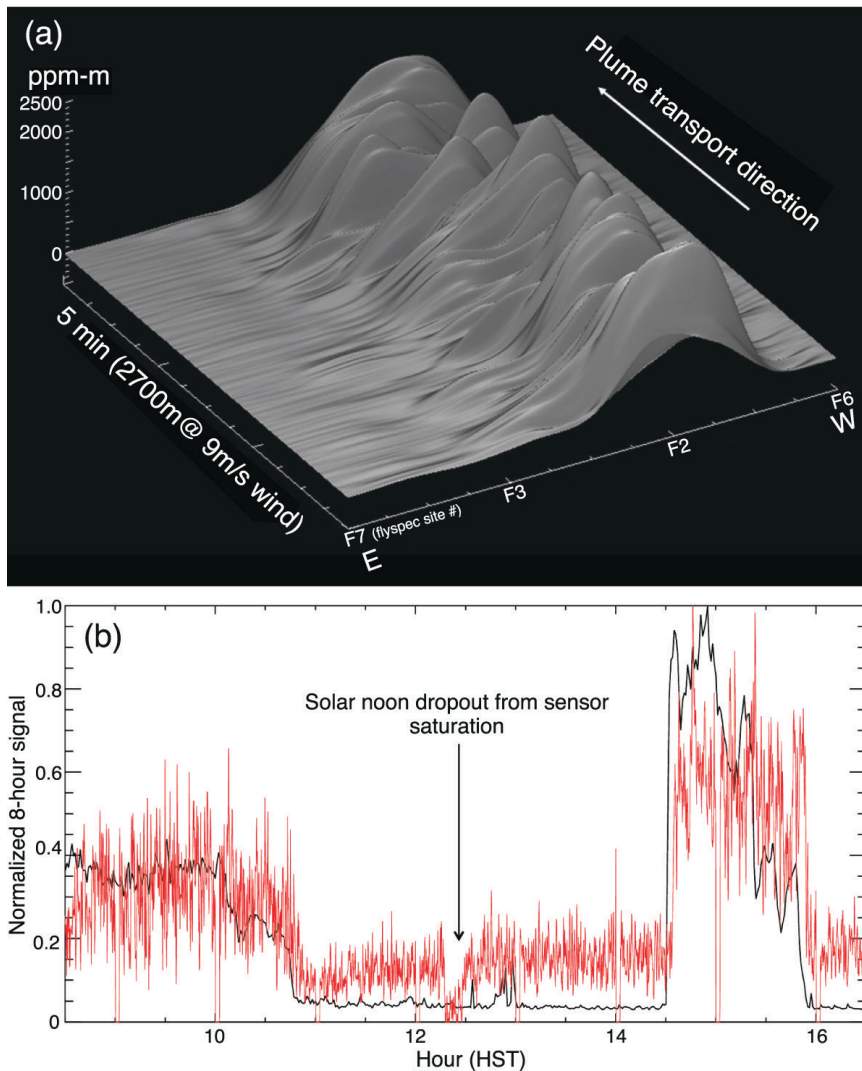


FIG. 6. (a) Plume SO₂ structure measured by the FLYSPEC array for a single 5-min period. (b) Plot of 10-m real-time seismic amplitude monitoring (RSAM) seismic signal (black) for 15 Aug 2012 with 10-s array SO₂ emission rate (red), both normalized to their maximum values. [Data courtesy USGS HVO.]

numerical model approach has been implemented as part of VMAP to forecast the dispersion of emissions from Kilauea volcano across the island of Hawaii and the other main Hawaiian Islands.

The dispersion model employed for this purpose is the Hybrid Single-Particle Lagrangian Integrated Trajectory model (HYSPLIT), version 4 (Draxler and Hess 1997, 1998),² hereafter Vog model. HYSPLIT was chosen for its low computational overhead to allow for operational forecast guidance to be made available to stakeholders and the public on a daily basis and in a timely way. The operational Vog model will soon transition to an ensemble mode that will

² Further detail regarding the HYSPLIT design and specifications can be found online (www.arl.noaa.gov/HYSPLIT_info.php).

allow uncertainties in the emissions and airflow to be modeled as probability distributions (e.g., Pattantyus and Businger 2014a). Ensemble prediction is even more computationally demanding. Moreover, for long-range transport of pollutants, intercomparison studies show that HYSPLIT is quite competitive with more comprehensive chemical models (e.g., Ryaboshapko et al. 2007), though the latter models include a more comprehensive description of other atmospheric processes than HYSPLIT. A more sophisticated sulfur chemistry module particular to Kilauea and the unique Hawaiian environment will be added to the Vog model in the near future as discussed in the last section of the paper. Vog model trajectory simulations require wind fields on sigma surfaces and surface pressure as input to the Vog model, which then performs time-integrated advection. Concentration and dispersion components of the Vog model require

moisture and temperature variables to compute the vertical diffusivity profile. Wind shear and horizontal deformation of the wind field are used to compute mixing. Because the Vog model lacks cloud water at this time, the conversion rate from SO₂ to sulfate aerosol was set to a constant rate of 1% per hour based on estimates of the half-life of SO₂ (Porter et al. 2002; McGonigle et al. 2004; Beirle et al. 2013). The model currently does not account for nucleation or coagulation microphysics.

The Vog model sets a plume height for volcanic emissions in the model as follows: most (85%) of the emissions are released at 300 and 700 m above the Pu'u Ō'ō and Halema'uma'u vents, respectively; 5% is released at the lowest model level; and 10% is released at 500 m. These values were arrived at

through empirical matching with surface observations. Because this is a static approach to a dynamic system, its limitations are recognized and improvements are being developed in the form of a dynamic plume model.

The Vog model disperses pollutants as 3D particles. A discrete number of particles are released at each time step based on forecast length and number of particles to be released per cycle (Draxler and Hess 1997; Pattantyus and Businger 2014b); 20,000 particles are released per cycle over 59 time steps (hours), resulting in approximately 339 particles released per time step. These particles are evenly distributed among 20 emission locations, such that during each time step approximately 17 particles are released from each source location. Each particle represents the mass of both SO₂ and sulfate (SO₄). In the particle implementation of the model, the dispersion process is represented by adding a turbulent component to the mean velocity obtained from the WRF Model. The specific approach used follows the one described by Fay et al. (1995). Based upon emission characteristics and the density of aerosols emanating from the source, the total mass of emissions is divided among the number of particles released. Each of these particulates is advected along a mean trajectory with a turbulent component added to represent the dispersive nature of the atmosphere. For additional details the reader is referred to Draxler and Hess (1997). In our case, initially the particles represent only the SO₂ concentration emanating from the source. However, particles still in the computational grid from the previous cycle are included in the grid for the new cycle.

The Vog model also performs wet and dry deposition calculations. The model calculates dry deposition (D_{dry}) as

$$D_{\text{dry}} = m\{1 - \exp[-\Delta t(V_d \Delta Z_p^{-1})]\}, \quad (1)$$

where m is mass, Δt is the time increment, V_d is the explicit deposition velocity, and Δz_p represents the depth of the pollutant layer (the lowest model layer). Dry deposition of sulfate aerosols was performed explicitly in this research, using 2.5 mm s⁻¹ estimated fall velocities for sulfate and 4.8 mm s⁻¹ for SO₂ (Rolph et al. 1992, 1993). These simple deposition velocities have performed adequately in the past (cf. Rolph et al. 1992, 1993). Therefore, in an effort to limit the computational overhead, this approach was adopted instead of the alternative of implementing resistance deposition calculations.

Wet removal represents a more viable deposition mechanism for vog aerosol. The majority of Hawaii's annual rainfall (up to 600 cm yr⁻¹) occurs on the

windward side, upwind of Kilauea's emission sources, because of orographic effects. Areas to the southwest of Kilauea, including South Point and inland Kona areas, have relatively less precipitation (50–200 cm yr⁻¹) (Giambelluca et al. 2013). The maximum rainfall along the Kona coast generally occurs with afternoon showers over upland areas associated with the diurnal sea-breeze circulation. Elevated aerosol concentrations along the Kona coast may decrease rainfall efficiency and increase cloud and rain acidity—conditions that can adversely impact agricultural crops such as coffee and tropical fruit; however, there is no published research confirming this hypothesis. At the moment there is no cloud water in the Vog model, so the wet deposition is parameterized based on an empirical approach. Gaseous SO₂ wet removal is described by Henry's constant = 1.24 molarity. Wet removal of sulfate particles is defined by nonzero values for the in-cloud and below-cloud parameters. In-cloud removal is defined as the ratio of the pollutant in air (grams per liter of air in the cloud layer) to that in rain (grams per liter) measured at the ground. Below-cloud removal is defined through a removal time constant.

The Vog model is run daily at 0000 and 1200 UTC for 60 h, with hourly output. The Vog model runs thus provide an effective 48-h forecast, because the meteorological input dataset introduces an ~12-h latency. Vog model output is a near-ground concentration of SO₂ and sulfate particles. The Vog model output employs the same color code as that used by the EPA air quality index (AQI) to distinguish the relative hazard levels in the model output (Fig. 7). The AQI is a generic index for reporting daily air quality and a modified version is also used by the Hawaii State Department of Health (DOH) for its short-term SO₂ advisory. The EPA calculates the AQI for five major air pollutants regulated by the Clean Air Act: i) ground-level ozone, ii) particulate matter, iii) carbon monoxide, iv) sulfur dioxide, and v) nitrogen dioxide. For each of these pollutants, the EPA has established national air quality standards to protect public health. Ground-level ozone and airborne particles are the two pollutants that are most ubiquitous and pose the greatest threat to human health in the continental United States. However, in 2010 the EPA promulgated a new, more stringent SO₂ air quality standard that is intended to improve public health (EPA 2010). The AQI level provides a gauge of the health effects that may result within a few hours or days of breathing air with a pollution concentration exceeding that AQI level. The vog model output, which provides hourly forecasts of hazard levels for SO₂ gas and sulfate particles, has been made available in real time to the public.

High-resolution wind fields and the WRF NWP model. To develop an accurate forecast of the trajectory and dispersion of the vog plume, the Vog model requires high-resolution wind fields and thermodynamic data as input. These data are provided by output from a numerical weather prediction (NWP) model. A new cluster at MKWC (Businger et al. 2002) has made possible high-resolution wind forecasts over the state of Hawaii produced by the WRF Model

(Klemp et al. 2007; Businger and Cherubini 2011, chapter 9), which provide the input for the Vog model.

The Local Analysis and Prediction System (LAPS; McGinley 1989; McGinley et al. 1991; Cherubini et al. 2006, 2008a,b) was adapted to Hawaii and the central North Pacific to assimilate available operational and custom weather data to produce local high-resolution analyses over the central North Pacific Ocean and the Hawaiian Islands. These data include atmospheric motion vector (AMV) data; satellite cloud and moisture data; global positioning system (GPS) precipitable water (PW) data; and local data from NOAA's Meteorological Assimilation Data Ingest System (MADIS), including Aircraft Communication, Addressing, and Reporting System (ACARS) data. Precipitable water can be estimated using the delay data from a ground-based GPS receiver (Bevis et al. 1992; Businger et al. 1996). Data from the relatively dense network of GPS receivers around the state of Hawaii are assimilated into LAPS. These data produce a better short-term forecast of cloud distribution and precipitation, which in turn provides better boundary conditions for the Vog model (Gutman and Benjamin 2001; Foster et al. 2003). More details about the implementation of WRF and LAPS in Hawaii can be found in Cherubini et al. (2006, 2008a,b).

The Advanced Research version of the WRF core was implemented at MKWC (Skamarock et al. 2005). WRF is a nonhydrostatic model with multiple nesting capabilities. The MKWC configuration encompasses three two-way nested domains, with horizontal resolution spacing of 15, 3, and 1 km that corresponds to a time step of 75, 25, and 5 s, respectively (Fig. 8). The

outermost domain covers a wide portion of the central Pacific area, the 3-km-resolution domain spans the main Hawaiian Islands, and the 1-km domain covers the island of Hawaii. WRF is a sigma-level model where 40 levels are used in the vertical. The vertical spacing is produced using terrain-following coordinates starting on the order of tens of meters for the levels nearest to the ground and gradually increases with height (Fig. 8). The model top

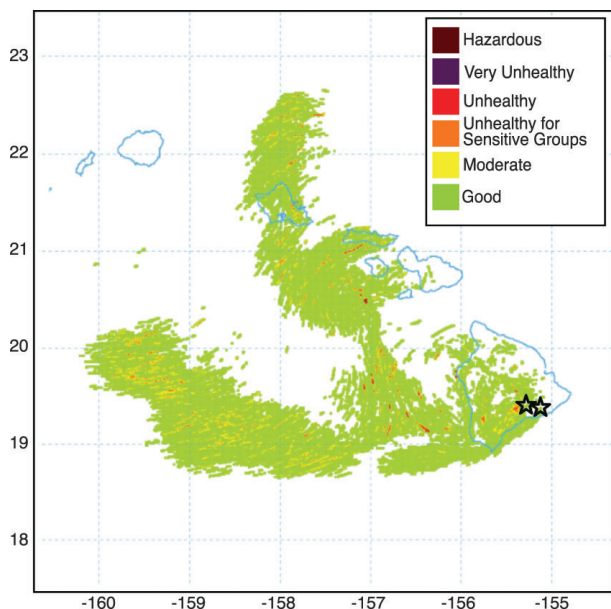


FIG. 7. Vog model 8-h forecast of sulfate aerosol concentration ($\mu\text{g m}^{-3}$) averaged between 0 and 100 m above ground level and integrated from 2200 to 2300 UTC 16 Apr 2013. Color scale shows EPA designations for six levels of health risk corresponding to the $\text{PM}_{2.5}$ AQI thresholds given in Table 1.

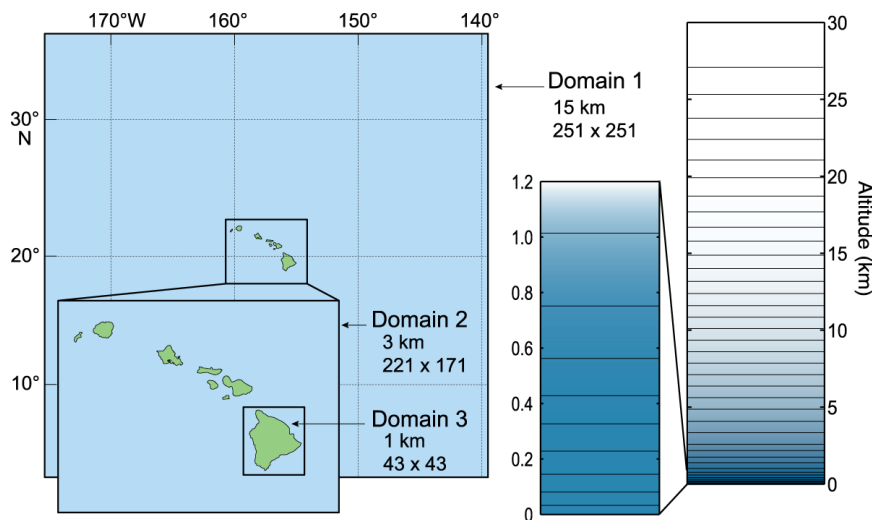


FIG. 8. WRF configuration showing three nested domains and grid resolution.

is fixed at 10 hPa, which corresponds to a height of ~25 km above ground level.

The WRF physics package used in the operational configuration includes i) the ice microphysics modeled using an approach by Hong et al. (2004); ii) the Kain–Fritsch cumulus convection scheme (Kain and Fritsch 1990, 1993) for the 15-km domain; (iii) the Mellor–Yamada–Janjić (MYJ) planetary boundary layer scheme (Janjić 2001), which solves the prognostic equation for the turbulence kinetic energy; and (iv) the longwave–shortwave radiation scheme of Mlawer et al. (1997). The WRF Model is run twice daily with 0000 and 1200 UTC initial conditions produced by LAPS. Boundary conditions are updated every 6 h using model output from the National Centers for Environmental Prediction Global Forecast System (NCEP GFS). More details about the implementation of WRF and LAPS in Hawaii can be found in Businger and Cherubini (2011).

The model is run on an eight-CPU quad-core Intel Xeon cluster at the University of Hawai‘i at Mānoa (UH). This small cluster contains 32 processors. However, it is a shared resource; thus, the computational constraints made the computationally efficient HYSPLIT a logical choice over more comprehensive models, such as the Community Multiscale Air Quality (CMAQ) model or WRF-Chem. The operational Vog model has a lag of one synoptic cycle (~12 h). This is because the WRF simulation used to force the model takes approximately 8–10 h to complete each cycle before the Vog model can start its own 1–3-h simulation and postprocessing.

VOG MODEL RESULTS AND VALIDATION.

Qualitative comparisons. Forecasting the presence or absence of the vog plume over locations within the state is one of the primary goals of VMAP. A qualitative comparison of the spatial distribution of SO₂ in satellite data from the Ozone Monitoring Instrument (OMI) on the National Aeronautics and Space Administration (NASA)’s *Aura* satellite and the graphical output from the Vog model is presented here for a case of prevailing northeasterly trade wind flow and for kona or southerly winds (Figs. 9 and 10). These images show that the position of the vog plume is well forecast over the island of Hawaii. The areas of higher observed concentration are qualitatively well captured by the model in terms of the location and pattern of the forecast distribution. The OMI observations represent total columnar SO₂ (DU), while the model represents only layer-averaged SO₂ concentrations from 0 to 100 m. This is not an apples-to-apples comparison, unfortunately, but OMI observations

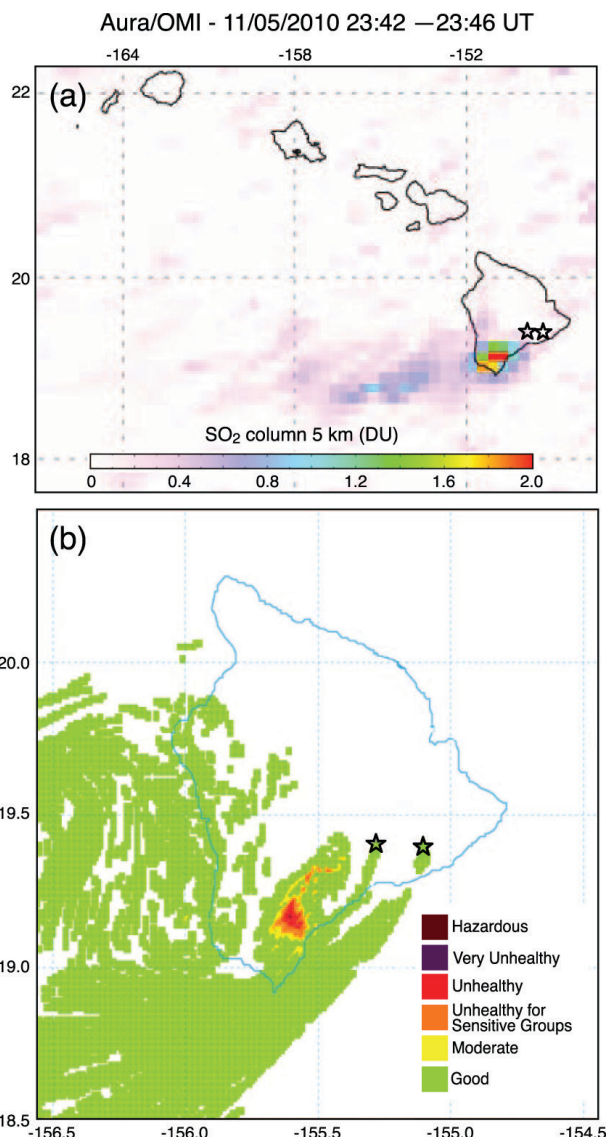


FIG. 9. (a) *Aura*-OMI satellite SO₂ column (DU) and (b) modeled ground-level sulfate concentration, valid at 2300–0000 UTC [1300–1400 Hawaii–Aleutian standard time (HST)] 5 Nov 2010 under prevailing northeasterly wind conditions.

represent one of the few options to observe the total SO₂ field as forecast by the Vog model. Forecasters at the National Weather Service (NWS) Weather Forecast Office (WFO) Honolulu have noted that the timing of the vog plume passage over Oahu under conditions of southeast flow is well forecast by the Vog model (R. Ballard 2012, personal communication) (e.g., Fig. 7). NWS forecasters are able to advise residents when vog will become present in the air over Honolulu and when the vog will likely retreat.

Quantitative model validation. Comparisons made between early Vog model forecasts of SO₂ and sulfate

aerosol concentrations and ground-based measurements allowed for an empirical adjustment of the vertical distribution of the emission input into the model to improve the model's accuracy. Following these early empirical adjustments, the Vog model was

kept in a "static mode" whereby no further changes were introduced. Once sufficient data were collected, a quantitative comparison could be conducted between the model forecast and observed values of ground-level SO₂ and PM_{2.5} for Pahala, Ocean View, and Kailua-Kona, obtained from the Hawaii State Department of Health. Observed values of SO₂ from Kilauea Visitor Center were obtained from the U.S. National Park Service. The time frame of the analysis is from 22 October 2010 to 27 August 2011.

The validation analysis uses 3-h-averaged data to ascertain and compare observed and forecast maximum AQI levels reached for each day over the 10-month period of stable model runs. The SO₂ AQI levels are defined by the Hawaii State Department of Health and provided in Table 1. Because the motivation for the VMAP project is to provide guidance regarding the health threat associated with the vog pollution concentrations, the AQI levels provide a meaningful and convenient way to bin the data. Three-hourly average data remove the highest frequency variability, which can contain noise both in the observations and the model output. The analysis focuses on the forecast levels for the following day, that is, the 12- to 36-h forecast window from the Vog model runs. Hourly model output was used in calculating the 3-h average values. Days for which either the observed or model data were missing were excluded from the analysis. Some model runs are missing due to missing WRF input to start the model, and occasional power outages or hardware issues for the cluster running the vog model result in other missing data. Since the whole system is run operationally, missing runs were never completed.

The PM_{2.5} sensors integrate all ambient aerosols—nonvolcanic salt, dust, pollen, etc.—that are not represented in the Vog model. Local industry, power plants, and vehicles produce nonvolcanic sources of SO₂ and sulfate aerosols in the Hawaiian environment. To account for these nonvolcanic sources in our validation analysis, a model forecast bias was calculated (Table 2). The bias calculation

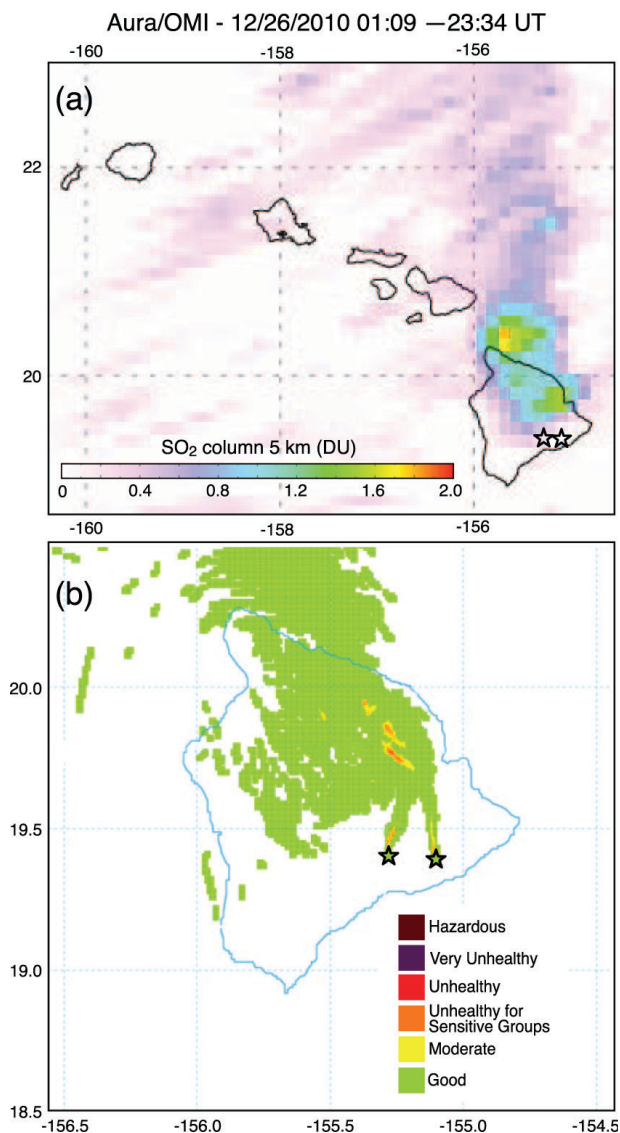


FIG. 10. As in Fig. 9, but at 2300–0000 UTC (1300–1400 HST) 25 Dec 2010 under southerly wind conditions.

TABLE 1. SO₂ (PPM) and particulate matter ($\mu\text{g m}^{-3}$) concentrations used to define the VMAP color codes. The SO₂ designations are consistent with those used by the Hawaii State Department of Health for their short-term SO₂ index. The EPA uses PM_{2.5} concentration thresholds for their 24-h AQI designations. Measurements are generally made 2 m above the surface.

| | 1 Good | 2 Moderate | 3 Unhealthy for sensitive groups | 4 Unhealthy | 5 Very unhealthy | 6 Hazardous |
|---|------------------------|------------|----------------------------------|-------------|------------------|-------------|
| SO ₂ (PPM) | 0–0.1 | 0.11–0.2 | 0.21–1.0 | 1.01–3.0 | 3.01–5.0 | >5.01 |
| PM _{2.5} (mg m ⁻³) | 1×10^{-8} –15 | 15.01–35 | 35.01–65 | 65.01–150 | 150.01–250 | >250.01 |

also allows for a reduction of systematic errors in the model. The bias was determined for each AQI level, pollutant (SO₂ or sulfate aerosol), and location by finding the average difference between the forecast value and the observed value for the entire time period for each observation station (Fig. 1). The dataset contains approximately 10 months of data, and AQI levels 3–6 were rarely observed. Therefore, levels 3–6 were combined into one category for bias calculations.

A background level of aerosol not associated with volcanic emissions can be seen in the surface observations when the winds blow the vog plume away from a particular sensor. Because PM_{2.5} measurements include nonvolcanic particulate, comparisons between model-forecast sulfate aerosol concentrations and measured PM_{2.5} include a negative bias due to the nonvolcanic background aerosol. Forecast values show a negative bias for AQI level 1 at all locations for both SO₂ and sulfate aerosol (Table 2). The largest negative bias in PM_{2.5} (of which sulfate is assumed to be the main component) was ~15 μg m⁻³ at Kailua-Kona, which may in part reflect local anthropogenic aerosol emissions from internal combustion engines and electricity generation. Forecast values for AQI level 2 and above, however, showed a positive bias for both SO₂ and sulfate aerosol at all locations in the study.

Closer inspection of model bias indicates a larger sulfate positive bias for AQI levels 2 and above for locations closer to the vent and a larger SO₂ bias for locations farther from the vent (Table 2). Currently, the Vog model does not explicitly model wet processes; instead, the conversion of SO₂ to sulfate aerosol is set in the model to a constant rate of 1% per hour. The bias pattern suggests that inclusion of a prognostic chemical model, within the Vog model, that takes into account the wet conversion of SO₂ to sulfate aerosol in cloud will improve this pattern of bias. In addition, the observed presence of primary sulfate in the plume at Kilauea's emission sources would be expected to result in a negative bias at monitoring sites close to vents, since this primary sulfate has not been included in the Vog model's initial condition to date.

A systematic model bias can be corrected a priori in the model forecast output once it is known, because the bias error tends to recur in a consistent pattern. It is important to note that the simple bias approach is applied here only as a step in assessing the utility of the Vog model at its current level of development. We are actively working to improve the model so that systematic errors and biases are reduced or eliminated. The next step in the analysis was to compare the

TABLE 2. Model bias for SO₂ in PPM and sulfate aerosol (μg m⁻³) for four observation sites on the island of Hawaii as a function of AQI level. Sulfate (PM_{2.5}) observations for Kilauea Visitor Center do not exist (DNE).

| | Visitor center | Pahala | Ocean View | Kailua-Kona |
|------------------------|----------------|--------|------------|-------------|
| SO₂ | | | | |
| AQI 1 | -0.01 | -0.04 | -0.01 | -0.00 |
| AQI 2 | 0.02 | 0.05 | 0.13 | 0.15 |
| AQI 3+ | 0.31 | 0.41 | 0.47 | NA |
| Sulfate aerosol | | | | |
| AQI 1 | DNE | -7.6 | -11.6 | -15.6 |
| AQI 2 | DNE | 14.5 | 9.5 | 5.0 |
| AQI 3+ | DNE | 89.2 | 91.9 | 64.1 |

bias-corrected forecast values and observed AQI level for each pollutant and location.

Forecast accuracy was estimated by taking the total number of forecast days and counting the total number of days where the forecast AQI category matched the observed AQI category. The forecast period was divided into 3-h increments, and hourly forecast values were then averaged per 3-h increment beginning at the start of each forecast period for the model run. The maximum 3-h value forecast for the day was compared to the observed 3-h-averaged maximum for the day.

The distribution of vog concentrations has some parallels to precipitation distributions in terms of variability and gradients. Therefore, a standard forecast accuracy analysis was conducted that is commonly used to assess the accuracy of precipitation forecasts. The analysis included the following quantities: perfect prognosis forecast (PPF), false alarm rate (FAR), and probability of detection (POD) (e.g., Klein et al. 1959). These variables will be defined further in the next section. Some FAR and POD values are not defined due to the limited dataset. While it is difficult to assess specific ideal values, it is certainly expected that PPF and POD values should exceed 0.5 and approach 1, and that FAR should be below 0.5 and approach 0.

The total number of forecast days for each category was compared to the total number of days where the forecast category matched the observed category. Kailua-Kona had the highest level of SO₂ forecast accuracy for all AQI levels (Fig. 11). Perhaps not surprisingly, results demonstrate greater sulfate aerosol forecast accuracy for AQI level 1 at all

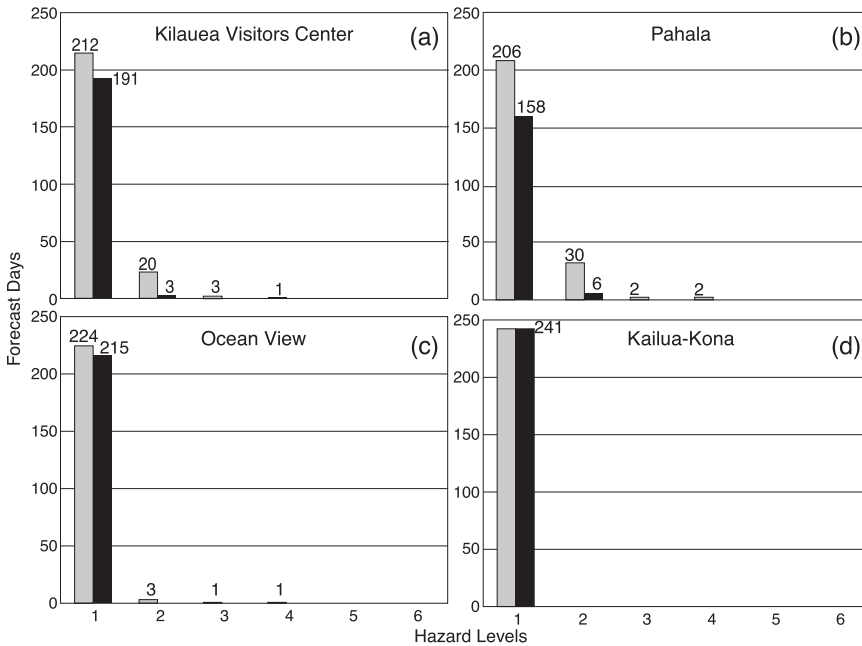


FIG. 11. Histogram of the total number of forecast days ($H + F$) for each SO_2 AQI level (gray) and the total number of days where the forecast level matched the observed (H) level (black) for (a) Kilauea Visitor Center, (b) Pahala, (c) Ocean View, and (d) Kailua-Kona. For explanation of H and F see Table 3.

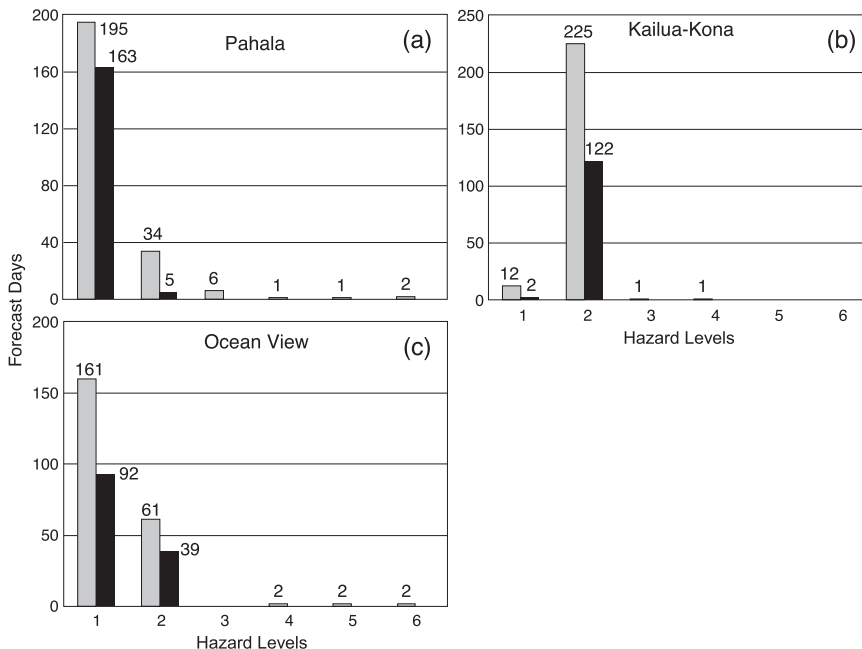


FIG. 12. As in Fig. 11, but for sulfate aerosol AQI level for (a) Pahala, (b) Kailua-Kona, and (c) Ocean View. For explanation of H and F see Table 4.

locations except Kailua-Kona, which shows greater accuracy for AQI level 2 than for AQI level 1 at that location (Fig. 12). Forecast values also show a few forecast outliers for SO_2 and sulfate for AQI level 4 and above for all locations except Kailua-Kona (Figs. 11 and 12).

not observed values (see Tables 3 and 4), which are used to calculate the perfect prognosis forecasts:

$$\begin{aligned} \text{PPF} &= (H+Z)/(H+F+M+Z), \\ \text{False Alarm Rate (FAR)} &= F/(F+Z), \text{ and} \\ \text{Probability of Detection (POD)} &= H/(H+M). \end{aligned} \quad (2)$$

The study also looked at how often the Vog model correctly forecast AQI levels ≥ 2 during days when observed values reached or exceeded AQI level 2. The data show that during days with observed values \geq AQI level 2, the Vog model forecast AQI levels of 2 or above just as frequently for SO_2 at Pahala as at the Kilauea Visitor Center and had zero verified forecasts at Ocean View (Fig. 13). For sulfate, Kailua-Kona had the highest number of days forecast that coincided with days of observed AQI levels ≥ 2 . These results may suggest that a more comprehensive chemical model component needs to be included in the Vog model that takes into account the wet conversion of SO_2 to sulfate in cloud and the inclusion of an initial sulfate aerosol load from the vent. Plume rise and vertical mixing in the model and real atmosphere may also be factors, especially nearer to the vent. These issues will be discussed in more detail in the “Conclusions and discussion” section.

Measures of skill commonly used to assess precipitation forecasts were applied next (Klein et al. 1959). In Eq. (2) H = forecast and observed, M = not forecast and observed, F = forecast and not observed, and Z = not forecast and

The results show high PPF values with most locations exceeding 80% SO₂ for AQI level 1 and levels ≥ 2 (Fig. 14). PPF values for locations where sulfate aerosol data exist are above 50% for both AQI level 1 and at or above 90% for levels ≥ 2 (Fig. 15). Because the AQI is for PM_{2.5} and not solely for sulfate aerosol, elimination of the bias prior to making the comparison here helps adjust for the nonsulfate component in PM_{2.5}. FAR values were low (5% or lower) for both SO₂ and sulfate aerosol at all locations for AQI level 2 and above, with the exception of Kailua-Kona sulfate (18%). FAR were higher (> 60%) for AQI level 1 sulfate and SO₂, except at Kailua-Kona (7%). POD values exceeded 80% for SO₂ AQI level 1 at all locations with much lower POD values for AQI levels ≥ 2. Note for SO₂ *H* and *M* = 0 at Ocean View and Kailua-Kona. POD values for sulfate aerosol AQI level 1 are near 80% at Pahala and Ocean View but only 2% at Kailua-Kona, while for AQI levels ≥ 2 POD increases with distance from Kilauea starting at 15% at Pahala to 35% at Ocean View and 92% at Kailua-Kona. This compares to the Storm Prediction Center forecast POD and FAR for significant severe weather of 49% and 31%, respectively (Roebber 2009).

The PPF values for sulfate aerosol were less accurate at locations farther away from the vent (Fig. 15). The PPF values in AQI level 1 decrease from 71% at Pahala to 53% at Kailua-Kona. A similar, albeit smaller, decrease can be seen in AQI level ≥ 2—from 94% to 90% at the same locations (Fig. 15). This pattern is reversed in SO₂, where Kailua-Kona has a PPF of 100% for AQI levels 1 and 2. The PPF decreases to 68% and 94% at Pahala for the same AQI levels, respectively, with slightly higher PPF values at the Kilauea Visitor Center (Fig. 14).

When looking at the overall pattern in the validation statistics, the highest forecast accuracy (POD) for both variables occurs at locations closest to the Kilauea Visitor Center and farthest away from the vent (Kailua-Kona) (Figs. 14 and 15). Locations between (Pahala and Ocean View) have lower forecast accuracy (POD). The lack of aqueous-phase chemistry in the model reduces the accuracy of the SO₂ to sulfate aerosol conversion rate. This deficiency in the model may help explain the lower accuracy in regions at moderate distances from the vent, where there is a more equal distribution of SO₂ and sulfate aerosol that are more sensitive to the conversion rate.

There is also a higher degree of accuracy in predicting SO₂ than sulfate aerosol. The POD values are consistently higher for SO₂ than for sulfate for each location. This difference may be explained in part by the fact that the model forecasts only sulfate aerosol concentrations, whereas the PM_{2.5} observations

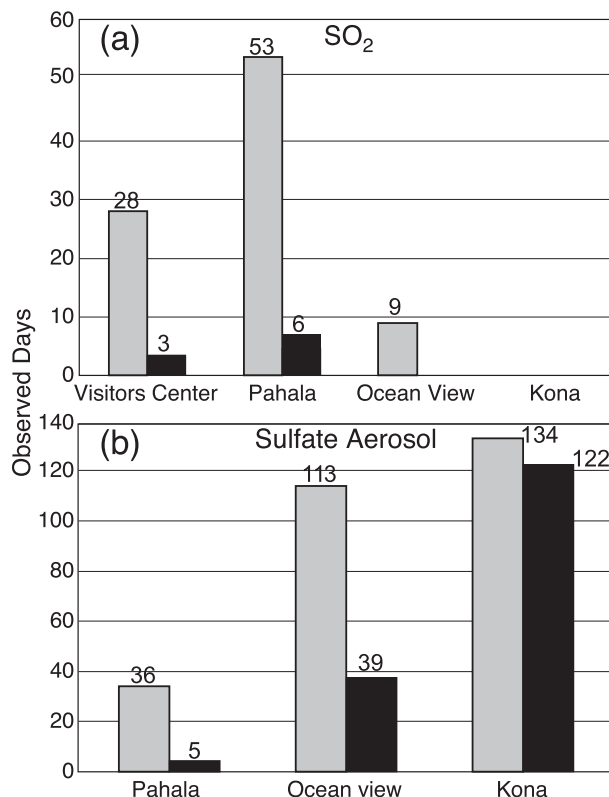


FIG. 13. Total number of observations (*H* + *M*) (gray) and number of forecasts that matched observations (*H*) (black) for AQI levels ≥ 2 for (a) SO₂ and (b) sulfate aerosol. Note that there were zero SO₂ observations for Kailua-Kona at AQI levels ≥ 2. For explanation of *H* and *M* see Tables 3 and 4.

collected by the Hawaii State Department of Health include nonsulfate aerosols (salt, dust, pollen, diesel exhaust, etc.).

CONCLUSIONS AND DISCUSSION. Results produced by the VMAP project demonstrate for the first time that by using SO₂ emissions observations for Kilauea volcano and the WRF wind-field output as input to a vog gas and particle dispersion model, it is possible to provide an operational forecast product that can help mitigate the effects of volcanic pollution for Hawaii residents, statewide. The public website that disseminates the VMAP vog forecast has experienced growing and widespread use, and is currently accessed ~200–1,000 times daily, depending on vog exposure. Image comparisons show that the extent of the vog plume is qualitatively well forecast over the island of Hawaii and that even the areas of higher observed concentration are qualitatively well captured by the model. The timing of the plume passage over downwind islands under southeast flow conditions is also well captured by the Vog model. By extension, when the

TABLE 3. Contingency table of forecast skill for SO₂ AQI; H = (forecast and observed), M = (not forecast and observed), F = (forecast and not observed), and Z = (not forecast and not observed values) for Pahala (PA), Ocean View (OV), Kailua-Kona (KN), and Kilauea Visitor Center (VC) for each AQI level. FCST = forecast.

| Pahala | | | PA AQI 1 | PA AQI 2 | PA AQI 3 | PA AQI 4 | PA AQI 5 | PA AQI 6 |
|------------------------|--------------|--------------|----------|----------|----------|----------|----------|----------|
| H | Forecast | Observed | 158 | 6 | 0 | 0 | 0 | 0 |
| F | Forecast | Not observed | 48 | 24 | 2 | 2 | 0 | 0 |
| M | Not forecast | Observed | 29 | 34 | 13 | 0 | 0 | 0 |
| Z | Not forecast | Not observed | 7 | 178 | 227 | 240 | 242 | 242 |
| Ocean View | | | OV AQI 1 | OV AQI 2 | OV AQI 3 | OV AQI 4 | OV AQI 5 | OV AQI 6 |
| H | Forecast | Observed | 215 | 0 | 0 | 0 | 0 | 0 |
| F | Forecast | Not observed | 9 | 3 | 1 | 1 | 0 | 0 |
| M | Not forecast | Observed | 5 | 9 | 0 | 0 | 0 | 0 |
| Z | Not forecast | Not observed | 0 | 217 | 228 | 228 | 229 | 229 |
| Kailua-Kona | | | KN AQI 1 | KN AQI 2 | KN AQI 3 | KN AQI 4 | KN AQI 5 | KN AQI 6 |
| H | Forecast | Observed | 241 | 0 | 0 | 0 | 0 | 0 |
| F | Forecast | Not observed | 0 | 0 | 0 | 0 | 0 | 0 |
| M | Not forecast | Observed | 0 | 0 | 0 | 0 | 0 | 0 |
| Z | Not forecast | Not observed | 0 | 241 | 241 | 241 | 241 | 241 |
| Kilauea Visitor Center | | | VC AQI 1 | VC AQI 2 | VC AQI 3 | VC AQI 4 | VC AQI 5 | VC AQI 6 |
| H | Forecast | Observed | 191 | 3 | 0 | 0 | 0 | 0 |
| F | Forecast | Not observed | 21 | 17 | 3 | 1 | 0 | 0 |
| M | Not forecast | Observed | 15 | 7 | 18 | 0 | 0 | 0 |
| Z | Not forecast | Not observed | 9 | 209 | 215 | 235 | 236 | 236 |

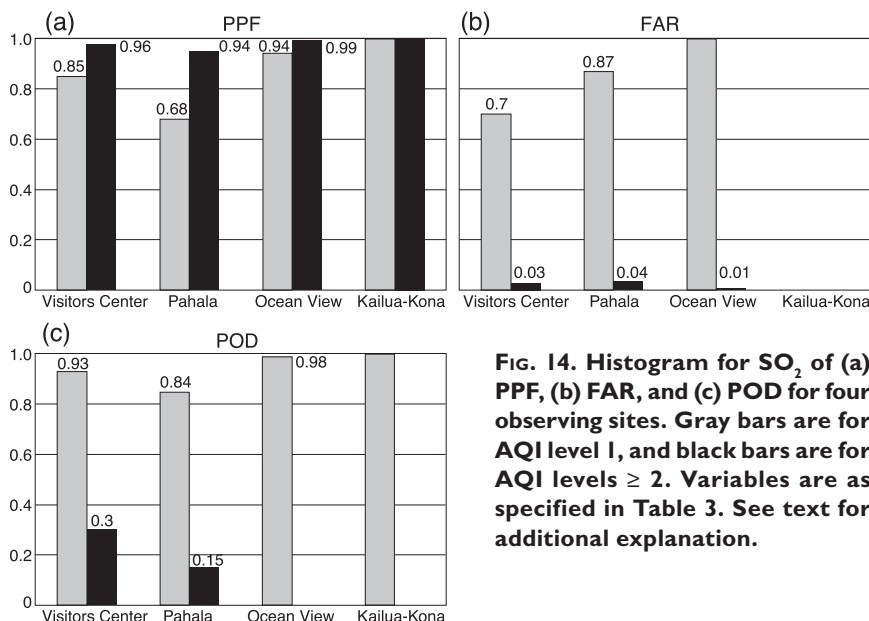


FIG. 14. Histogram for SO₂ of (a) PPF, (b) FAR, and (c) POD for four observing sites. Gray bars are for AQI level 1, and black bars are for AQI levels ≥ 2. Variables are as specified in Table 3. See text for additional explanation.

user can plan on the likelihood of elevated sulfate aerosols and/or SO₂.

The quantitative analysis of Vog model performance at four sites on the island of Hawaii shows that the model accurately forecasts AQI levels more than 70% of the time for SO₂ at locations closest and farthest from Kilauea's summit (Kilauea Visitor Center and Kailua-Kona, respectively) with poorer agreement for forecast sulfate aerosol at sites with more equal distributions of both pollutants (Pahala and Ocean View). These results

Vog model predicts that the plume position will be over a particular region, as highlighted by the model graphical output of the forecast vog concentration, a

support the suggestion that much of the negative bias for AQI level 1 is a result of ambient sulfates or aerosols and that the positive bias for AQI level

| TABLE 4. As in Table 3, but for sulfate aerosol (SO ₄ ²⁻). | | | | | | | | |
|---|--------------|--------------|----------|----------|----------|----------|----------|----------|
| Pahala | | | PA AQI 1 | PA AQI 2 | PA AQI 3 | PA AQI 4 | PA AQI 5 | PA AQI 6 |
| H | Forecast | Observed | 163 | 5 | 0 | 0 | 0 | 0 |
| F | Forecast | Not observed | 32 | 29 | 6 | 1 | 1 | 2 |
| M | Not forecast | Observed | 38 | 29 | 2 | 0 | 0 | 0 |
| Z | Not forecast | Not observed | 6 | 176 | 231 | 238 | 238 | 237 |
| Ocean View | | | OV AQI 1 | OV AQI 2 | OV AQI 3 | OV AQI 4 | OV AQI 5 | OV AQI 6 |
| H | Forecast | Observed | 92 | 39 | 0 | 0 | 0 | 0 |
| F | Forecast | Not observed | 69 | 22 | 0 | 2 | 2 | 2 |
| M | Not forecast | Observed | 24 | 73 | 1 | 0 | 0 | 0 |
| Z | Not forecast | Not observed | 44 | 95 | 228 | 227 | 227 | 227 |
| Kailua-Kona | | | KN AQI 1 | KN AQI 2 | KN AQI 3 | KN AQI 4 | KN AQI 5 | KN AQI 6 |
| H | Forecast | Observed | 2 | 122 | 0 | 0 | 0 | 0 |
| F | Forecast | Not observed | 10 | 103 | 1 | 1 | 0 | 0 |
| M | Not forecast | Observed | 103 | 11 | 0 | 0 | 0 | 1 |
| Z | Not forecast | Not observed | 124 | 3 | 238 | 238 | 239 | 238 |

2 and above can be largely attributed to model error resulting from chemical conversion rates and from the lack of aqueous-phase chemistry in the model. Additionally, a recent field campaign produced measurements of nonnegligible primary aerosols released at the vent (Mather et al. 2012). Aerosol measurements at the vent are not operationally available at this time, but in the future it may be possible to estimate the aerosol emission as a percentage of the SO₂ gas emission and to include it in the model input.

Since the time that the forecast model first became operational, source parameter improvements have been made by implementing nearly continuous SO₂ emission rate measurements at Kilauea's summit during daylight hours.

Future work. It is clear from the model verification results that the model forecast accuracy can be further improved. There are several steps that we plan to undertake to produce a more accurate forecast. Perhaps the most important step is to better characterize the conversion rate from SO₂ gas to

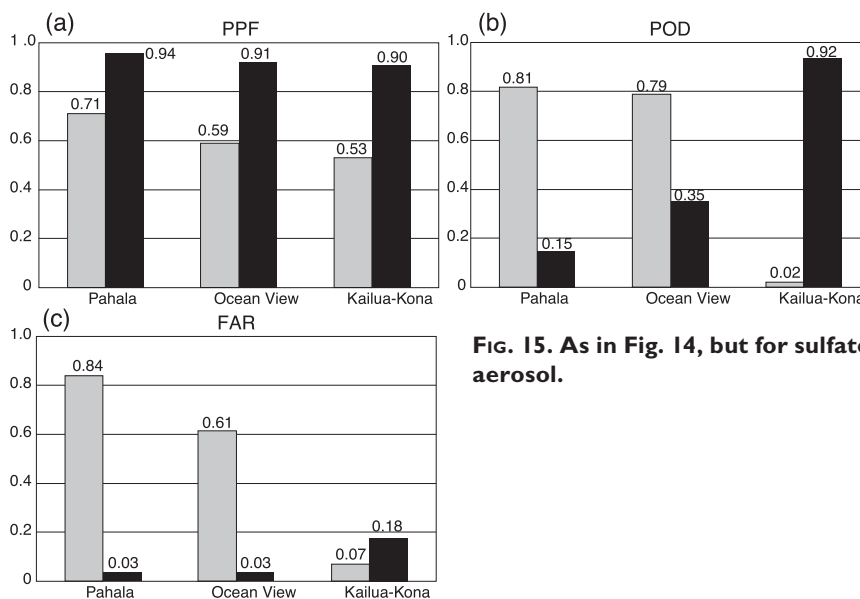


FIG. 15. As in Fig. 14, but for sulfate aerosol.

sulfate aerosols and to explore the release of primary particles at the vent (e.g., Mather et al. 2012).

In the future, the Vog model will be able to estimate the clear-air oxidation of SO₂ to sulfate by assuming a modulated concentration of the hydroxyl radical, OH, throughout the day, resulting in a conversion rate that peaks at noon and reaches a minimum at night. The gas-phase oxidation of SO₂ by OH is too slow to explain the observed atmospheric lifetimes of hours to 1–2 days. Implementation of the aqueous-phase pathway in the Vog model is required. We propose the inclusion of a variable three-dimensional field of liquid water content obtained from the WRF Model output to

improve the simulation of the geographical distribution of SO_2 and SO_4^{2-} downwind of Kilauea. There is a flux of water vapor at the Kilauea vents that also must be considered. In the future, the magnitude of this flux will be estimated so that it can be included in the initial condition of the model and be accounted for by the aqueous component of the improved Vog model.

The approach described above is simplified relative to explicit atmospheric chemistry and dispersion models (cf. Foley et al. 2010; Grell et al. 2005). The addition of chemistry to Eulerian numerical weather prediction models substantially increases the computational burden; however, a sulfur chemistry scheme developed for HYSPLIT proves very economical (Rolph et al. 1992, 1993). Only the dominant gaseous- and aqueous-phase pathways are considered for SO_2 to SO_4 conversion, and reactant concentrations are not explicitly solved. Preliminary benchmark testing suggests implementation of sulfur chemistry in this manner would increase computation time by 10–30 min depending on particle residence time (meteorological conditions). An Eulerian solution using the current grid would result in 9×10^5 chemistry computations at each time step, whereas following 2×10^4 discrete particles adds considerably fewer chemistry computations. Solving explicit chemistry for our application would therefore be computationally prohibitive given the operational constraints.

The height of the plume is another important initial condition for the Vog dispersion model. Using stereocameras it is possible to determine the location of cloud edge features at a particular time, which would allow us to estimate the rise of the volcano plume and associated wind shear (Porter and Cao 2009). Plume speed is estimated using a series of UV spectrometers (Williams-Jones et al. 2006), and these velocity data can be compared with the stereocamera approach and available surface wind data. Vog plume data collected by the stereocamera system can be used to validate a plume-rise algorithm, forced with a heat flux term for each source location, to provide a dynamic emission plume for the updated Vog model.

Another opportunity for Vog model improvement is to develop an ensemble model approach in which the Vog model is run in parallel with multiple meteorological model grids. The advantage of this approach is that the uncertainty caused by initial conditions, physics parameterizations, and turbulent closure schemes can be constrained because the ensemble output allows us to calculate the probability that a certain concentration will be exceeded at a location (Draxler 2003; Pattantyus and Businger 2014a). A separate workstation is now available to produce ensemble forecasts, which will

require significantly more computational resources than are available in the current system. The model is scalable and the ensemble will consist of 27 members. Given 27 processors the ensemble can be produced in the same time as the operational model; however, postprocessing output will require added time.

After updates to the UH Vog model initialization and chemistry, an intercomparison study with CMAQ and WRF-Chem will be undertaken to gauge the forecast performance of the Vog model against more comprehensive chemical dispersion models. Of interest are the effects of turbulence and diffusion parameterizations and sulfur chemistry routines in forecast quality. Forecast benchmarking will also be performed between the models using a standard grid over the island of Hawaii.

It is anticipated that with all these improvements, the utility of the Vog model output will continue to increase to the advantage of Hawaii's 1.4 million residents who actively live and work in the shadow of Kilauea volcano.

ACKNOWLEDGMENTS. We are grateful to Ryan Lyman and Roland Draxler for their technical support and encouragement and to Nancy Hulbert, who helped draft the final figures. We also thank Dr. C. Kern and the anonymous reviewers for their thoughtful comments on earlier drafts of the manuscript. The research was supported by the USGS under Grant G10AC00035, by NOAA under Grant NA11NMF4320128, and by the NSF under Grant number 1108569.

REFERENCES

- Barsotti, S. and A. Neri, 2008: The VOL-CALPUFF model for atmospheric ash dispersal: 2. Application to the weak Mt. Etna plume July 2001. *J. Geophys. Res.*, **113**, B03209, doi:10.1029/2006JB004624.
- Beirle, S., C. Horman, M. Penning de Vries, S. Dorner, C. Kern, and T. Wagner, 2013: Estimating the volcanic emission rate and atmospheric lifetime of SO_2 from space: A case study for Kilauea volcano, Hawai'i. *Atmos. Chem. Phys. Discuss.*, **13**, 28 695–28 727, doi:10.5194/acpd-13-28695-2013.
- Bevis, M., S. Businger, T. A. Herring, C. Rocken, R. A. Anthes, and R. H. Ware, 1992: GPS meteorology: Remote sensing of atmospheric water vapor using the global positioning system. *J. Geophys. Res.*, **97**, 15 787–15 801, doi:10.1029/92JD01517.
- Businger, S., and T. Cherubini, Eds., 2011: *Seeing Clearly: The Impact of Atmospheric Turbulence on the Propagation of Extraterrestrial Radiation*. VBW Publishing, 212 pp.
- , and Coauthors, 1996: The promise of GPS in atmospheric monitoring. *Bull. Amer. Meteor. Soc.*,

- 77, 5–18, doi:10.1175/1520-0477(1996)077<0005:TPOGIA>2.0.CO;2.
- , R. McLaren, R. Ogasawara, D. Simons, and R. J. Wainscoat, 2002: Starcasting. *Bull. Amer. Meteor. Soc.*, **83**, 858–871, doi:10.1175/1520-0477(2002)083<0858:S>2.3.CO;2.
- Casadevall, T. J., J. B. Stokes, L. P. Greenland, L. L. Malinconico, J. R. Casadevall, and B. T. Furukawa, 1987: SO₂ and CO₂ emission rates at Kilauea volcano, 1979–1984. *Volcanism in Hawaii: Papers to commemorate the 75th anniversary of the founding of the Hawaiian Volcano Observatory*, R. W. Decker, T. L. Wright, and P. H. Stauffer, Eds., USGS Prof. Paper 1350, Vol. 1, 771–780.
- Cherubini, T., S. Businger, C. Velden, and R. Ogasawara, 2006: The impact of satellite-derived atmospheric motion vectors on mesoscale forecasts over Hawaii. *Mon. Wea. Rev.*, **134**, 2009–2020, doi:10.1175/MWR3163.1.
- , —, R. Lyman, and M. Chun, 2008a: Modeling optical turbulence and seeing over Mauna Kea. *J. Appl. Meteor. Climatol.*, **47**, 1140–1155, doi:10.1175/2007JAMC1487.1.
- , —, —, and —, 2008b: Modeling optical turbulence and seeing over Mauna Kea: Verification and algorithm refinement. *J. Appl. Meteor. Climatol.*, **47**, 3033–3043, doi:10.1175/2008JAMC1839.1.
- Colette, A., and Coauthors, 2011: Assessing in near real time the impact of the April 2010 Eyjafallajökull ash plume on air quality. *Atmos. Environ.*, **24**, 1217–1221, doi:10.1016/j.atmosenv.2010.09.064.
- Draxler, R. R., 2003: Evaluation of an ensemble dispersion calculation. *J. Appl. Meteor.*, **42**, 308–317, doi:10.1175/1520-0450(2003)042<0308:EOAEDC>2.0.CO;2.
- , and G. D. Hess, 1997: Description of the HY-SPLIT_4 modelling system. NOAA Tech. Memo. ERL ARL-224, 27 pp.
- , and —, 1998: An overview of the HY-SPLIT_4 modelling system for trajectories, dispersion and deposition. *Aust. Meteor. Mag.*, **47**, 295–308.
- Elias, T., 1992: The effects of volcanic emissions on ambient air quality in Hawaii Volcanoes National Park. *Proc. Earthquake, Tsunami, and Volcano Hazards Seminar*, Hilo, HI, University of Hawaii at Hilo.
- , and A. J. Sutton, 2002: Sulfur dioxide emission rates of Kilauea Volcano, Hawai‘i, an update: 1998–2001. USGS Open-File Rep. 02-460, 29 pp.
- , and —, 2007: Sulfur dioxide emission rates from Kilauea Volcano, Hawai‘i, an update: 2002–2006. USGS Open-File Rep. 2007-1114, Version 1.0, 37 pp.
- , and —, 2012: Sulfur dioxide emission rates from Kilauea Volcano, Hawai‘i, 2007–2010. USGS Open-File Rep. 2012-1107, 25 pp.
- , —, J. B. Stokes, and T. J. Casadevall, 1998: Sulfur dioxide emission rates of Kilauea Volcano, Hawai‘i, 1979–1997. USGS Open-File Rep. 98-462, Version 1. [Available online at <http://pubs.usgs.gov/of/1998/of98-462/>.]
- , —, C. Oppenheimer, K. A. Horton, H. Garbeil, V. Tsanev, A. J. S. McGonigle, and G. Williams-Jones, 2006: Comparison of COSPEC and two miniature ultraviolet spectrometer systems for SO₂ measurements using scattered sunlight. *Bull. Volcanol.*, **68**, 313–322.
- , —, J. P. Kauahikaua, J. D. Ray, and J. L. Babb, 2009: Ambient air quality effects of the 2008–2009 Halema‘uma‘u eruption on the Island of Hawai‘i. *Eos, Trans. Amer. Geophys. Union*, **90** (Fall Meeting Suppl.), Abstract V43G-2337.
- EPA, 2010: Revisions to the primary national ambient air quality standard, monitoring network, and data reporting requirements for sulfur dioxide. Fact Sheet, 6 pp. [Available online at www.epa.gov/airquality/sulfurdioxide/pdfs/20100602fs.pdf.]
- Fast, J. D., and Coauthors, 2014: Modeling regional aerosol and aerosol precursor variability over California and its sensitivity to emissions and long-range transport during the 2010 CalNex and CARES campaigns. *Atmos. Chem. Phys.*, **14**, 10 013–10 060, doi:10.5194/acp-14-10013-2014.
- Favelli, M., F. MAzzarini, M. T. Pareschi, and E. Boschi, 2004: Role of local wind circulation in plume monitoring at Mt. Etna volcano (Sicily): Insights from a mesoscale numerical model. *Geophys. Res. Lett.*, **31**, L09105, doi:10.1029/2003GL019281.
- Fay, B., H. Glaab, I. Jacobsen, and R. Schrodin, 1995: Evaluation of Eulerian and Lagrangian atmospheric transport models at the Deutscher Wetterdienst using ANATEX surface tracer data. *Atmos. Environ.*, **29**, 2485–2497, doi:10.1016/1352-2310(95)00144-N.
- Foley, K. M., and Coauthors, 2010: Incremental testing of the Community Multiscale Air Quality (CMAQ) modeling system version 4.7. *Geosci. Model Dev.*, **3**, 205–226, doi:10.5194/gmd-3-205-2010.
- Forkel, R., A., and Coauthors, 2015: Analysis of the WRF-Chem contributions to AQMEII phase2 with respect to aerosol radiative feedbacks on meteorology and pollutant distributions. *Atmos. Environ.*, **115**, 630–645, doi:10.1016/j.atmosenv.2014.10.056.
- Foster, J., M. Bevis, Y.-L. Chen, S. Businger, and Y. Zhang, 2003: The Ka‘u storm (November 2000): Imaging precipitable water using GPS. *J. Geophys. Res.*, **108**, 4585, doi:10.1029/2003JD003413.

- Giambelluca, T. W., Q. Chen, A. G. Frazier, J. P. Price, Y.-L. Chen, P.-S. Chu, J. K. Eischeid, and D. M. Delporte, 2013: Online rainfall atlas of Hawai'i. *Bull. Amer. Meteor. Soc.*, **94**, 313–316, doi:10.1175/BAMS-D-11-00228.1.
- Grell, G. A., S. E. Peckham, R. Schmitz, S. A. McKeen, G. Frost, W. C. Skamarock, and B. Eder, 2005: Fully coupled online chemistry within the WRF model. *Atmos. Environ.*, **39**, 6957–6975, doi:10.1016/j.atmosenv.2005.04.027.
- Gutman, S. I., and S. G. Benjamin, 2001: The role of ground-based GPS meteorological observations in numerical weather prediction. *GPS Solutions*, **4**, 16–24, doi:10.1007/PL00012860.
- Heinhold, B., I. Tegen, R. Wolke, A. Ansmann, I. Mattis, A. Minikin, U. Schumann, and B. Weinzierl, 2012: Simulations of the 2010 Eyjafjallajökull volcanic ash dispersal over Europe using COSMO-MUSCAT. *Atmos. Environ.*, **48**, 195–204, doi:10.1016/j.atmosenv.2011.05.021.
- Hong, S.-Y., J. Dudhia, and S.-H. Chen, 2004: A revised approach to ice microphysical processes for the bulk parameterization of clouds and precipitation. *Mon. Wea. Rev.*, **132**, 103–120, doi:10.1175/1520-0493(2004)132<0103:ARATIM>2.0.CO;2.
- Horton, K. A., J. Porter, P. Mouginiis-Mark, C. Oppenheimer, and H. Garbeil, 2003: Apparatus for measuring radiation and method of use. U.S. Patent 7,148,488, filed 13 June 2003, and issued 12 December 2006.
- , G. Williams-Jones, H. Garbeil, T. Elias, A. J. Sutton, P. Mouginiis-Mark, J. N. Porter, and S. Clegg, 2006: Real-time measurement of volcanic SO₂ emissions: Validation of a new UV correlation spectrometer (FLYSPEC). *Bull. Volcanol.*, **68**, 323–327, doi:10.1007/s00445-005-0014-9.
- , H. Garbeil, A. J. Sutton, T. Elias, and S. Businger, 2012: Early monitoring results from the Halema'ūma'ū vog measurement and prediction FLYSPEC array. *Extended Abstracts, AGU Chapman Conf. on Hawaiian Volcanoes: From Source to Surface*, Waikoloa, HI, Amer. Geophys. Union, TH-34. [Available online at <http://hilo.hawaii.edu/~kenhon/HawaiiChapman/documents/1HawaiiChapmanAbstracts.pdf>]
- Hurley, P., 1994: PARTPUFF—A Lagrangian particle-puff approach for plume dispersion modeling applications. *J. Appl. Meteor.*, **33**, 285–294, doi:10.1175/1520-0450(1994)033<0285:PLPPAF>2.0.CO;2.
- Im, U., and Coauthors, 2015: Evaluation of operational on-line-coupled regional air quality models over Europe and North America in the context of AQMEII phase 2. Part I: Ozone, *Atmos. Environ.*, **115**, 404–420, doi:10.1016/j.atmosenv.2014.09.042.
- Janjić, Z. I., 2001: Nonsingular implementation of the Mellor–Yamada level 2.5 scheme in the NCEP Meso model. NCEP Office Note 437, 61 pp.
- Kain, J. S., and J. M. Fritsch, 1990: A one-dimensional entraining/detraining plume model and its application in convective parameterization. *J. Atmos. Sci.*, **47**, 2784–2802, doi:10.1175/1520-0469(1990)047<2784:AODEPM>2.0.CO;2.
- , and —, 1993: Convective parameterization for mesoscale models: The Kain–Fritsch scheme. *The Representation of Cumulus Convection in Numerical Models*, Meteor. Monogr., No. 46, Amer. Meteor. Soc., 246 pp.
- Kern, C., T. Deutschmann, C. Werner, A. J. Sutton, T. Elia, and P. J. Kelly, 2012: Improving the accuracy of SO₂ column densities and emission rates obtained from upward-looking UV-spectroscopic measurements of volcanic plumes by taking realistic radiative transfer into account. *J. Geophys. Res.*, **117**, D20302, doi:10.1029/2012JD017936.
- Klein, W. H., B. M. Lewis, and I. Enger, 1959: Objective prediction of five-day mean temperature during winter. *J. Meteor.*, **16**, 672–682, doi:10.1175/1520-0469(1959)016<0672:OPOFDM>2.0.CO;2.
- Kleinman, M. T., 1995: Health effects of inhaled particles and acid sulfate aerosols. *Proc. Vog and Laze Seminar*, Honolulu HI., Hawaii State Department of Health.
- Klemp, J. B., W. C. Skamarock, and J. Dudhia, 2007: Conservative split-explicit time integration methods for the compressible nonhydrostatic equations. *Mon. Wea. Rev.*, **135**, 2897–2913, doi:10.1175/MWR3440.1.
- Kodama, K. R., and S. Businger, 1998: A brief overview of weather and forecasting in the Pacific region of the National Weather Service. *Wea. Forecasting*, **13**, 523–546, doi:10.1175/1520-0434(1998)013<0523:WAFKIT>2.0.CO;2.
- Leopold, L. B., 1949: The interaction of trade wind and sea breeze, Hawaii. *J. Meteor.*, **6**, 312–320, doi:10.1175/1520-0469(1949)006<0312:TIOOTWA>2.0.CO;2.
- Longo, B. M., 2013: Adverse health effects associated with increased activity at Kilauea volcano: A repeated population-based survey. *ISRN Public Health*, **2013**, 475962, doi:10.1155/2013/475962.
- , W. Yang, J. B. Green, F. L. Crosby, and V. L. Crosby, 2010: Acute health effects associated with exposure to volcanic air pollution (vog) from increased activity at Kilauea Volcano in 2008. *J. Toxicol. Environ. Health*, **73**, 1370–1381, doi:10.1080/15287394.2010.497440.
- Mannino, D. M., S. M. Ruben, and F. C. Holschuh, 1995: Weekly variability of emergency room visits for asthma in Hilo, Hawai'i, 1981–1991. *Proc. Vog*

- and Laze Seminar, Honolulu HI., Hawaii State Department of Health.
- Mather, T., and Coauthors, 2012: Halogens and trace metal emissions from the ongoing 2008 summit eruption of Kilauea volcano, Hawai'i. *Geochim. Cosmochim. Acta*, **83**, 292–323, doi:10.1016/j.gca.2011.11.029.
- Matthias, V., and Coauthors, 2012: The ash dispersion over Europe during the Eyjafjallajökull eruption—Comparison of CMAQ simulations to remote sensing and air-borne in-situ observations. *Atmos. Environ.*, **48**, 184–194, doi:10.1016/j.atmosenv.2011.06.077.
- McGinley, J. A., 1989: The local analysis and prediction system. Preprints, *12th Conf. on Weather Analysis and Forecasting*, Monterey, CA, Amer. Meteor. Soc., 15–20.
- , S. C. Albers, and P. A. Stamus, 1991: Validation of a convective index as defined by a real-time local analysis system. *Wea. Forecasting*, **6**, 337–356, doi:10.1175/1520-0434(1991)006<0337:VOACCI>2.CO;2.
- McGonigle, A. J. S., P. Delmelle, C. Oppenheimer, V. I. Tsanev, T. Delfosse, G. Williams-Jones, K. Horton, and T. A. Mather, 2004: SO₂ depletion in tropospheric volcanic plumes. *Geophys. Res. Lett.*, **31**, L13201, doi:10.1029/2004GL019990.
- Mlawer, E. J., S. J. Taubman, P. D. Brown, M. J. Iacono, and S. A. Clough, 1997: Radiative transfer for inhomogeneous atmosphere: RRTM, a validated correlated-k model for the longwave. *J. Geophys. Res.*, **102**, 16 663–16 682, doi:10.1029/97JD00237.
- Morrow, J. W., 1991: The atmospheric fate of sulfur gases from Kilauea volcano. *Proc. Vog and Laze Seminar*, Honolulu HI., Center for the Study of Active Volcanoes.
- Nadeau, P. A., and Coauthors, 2011: High temporal resolution SO₂ emission rate data as part of a multi-parameter approach to studying summit vent activity at Kilauea volcano. *2011 Fall Meeting*, San Francisco, CA, Amer. Geophys. Union, Abstract V41A-2487.
- Palma, J. L., E. S. Calder, D. Basualto, S. Blake, and D. A. Rothery, 2008: Correlations between SO₂ flux, seismicity, and outgassing activity at the open vent of Villarrica volcano, Chile. *J. Geophys. Res.*, **113**, B10201, doi:10.1029/2008JB005577.
- Palmer, K. F., and D. Williams, 1975: Optical constants of sulfuric acid: Application to the clouds of Venus? *Appl. Opt.*, **14**, 208–219, doi:10.1364/AO.14.000208.
- Pattantyus, A., and S. Businger, 2014a: Ensemble forecasting of volcanic emissions in Hawai'i. *Ann. Geophys.*, **57**, doi:10.4401/ag-6607.
- , and —, 2014b: On the interaction of Tropical Cyclone Flossie and emissions from Hawai'i's Kilauea volcano. *Geophys. Res. Lett.*, **41**, 4082–4089, doi:10.1002/2014GL060033.
- Perner, D., and U. Platt, 1980: Detection of nitrous acid in the atmosphere by differential optical absorption. *Geophys. Res. Lett.*, **7**, 1053–1056, doi:10.1029/GL007i012p01053.
- Perrone, M. R., F. De Tomasi, A. Stohl, and N. I. Kristiansen, 2012: Characterization of Eyjafjallajökull volcanic aerosols over Southeastern Italy. *Atmos. Chem. Phys. Discuss.*, **12**, 15 301–15 335, doi:10.5194/acpd-12-15301-2012.
- Platt, U., 1994: Differential optical absorption spectroscopy (DOAS). *Air Monitoring by Spectroscopic Techniques*, M. W. Sigrist, Ed., Chemical Analysis Series, Vol. 127, Wiley, 27–84.
- Porter, J. N., and A. D. Clarke, 1997: Aerosol size distribution models based on in situ measurements. *J. Geophys. Res.*, **102**, 6035–6045, doi:10.1029/96JD03403.
- , and G. X. Cao, 2009: Using ground-based stereo cameras to derive cloud-level wind fields. *Opt. Lett.*, **34**, 2384–2386, doi:10.1364/OL.34.002384.
- , and Coauthors, 2002: Sun photometer and lidar measurements of the plume from the Hawaii Kilauea Volcano Pu'u O'o vent: Aerosol flux and SO₂ lifetime. *Geophys. Res. Lett.*, **29**, doi:10.1029/2002GL014744.
- Roebber, P. J., 2009: Visualizing multiple measures of forecast quality. *Wea. Forecasting*, **24**, 601–608.
- Rolph, G. D., R. R. Draxler, and R. G. de Pena, 1992: Modeling sulfur concentrations and depositions in the United States during ANATEX. *Atmos. Environ.*, **26**, 73–93, doi:10.1016/0960-1686(92)90262-J.
- , —, and —, 1993: The use of model-derived and observed precipitation in long-term sulfur concentration and deposition modeling. *Atmos. Environ.*, **27A**, 2017–2037, doi:10.1016/0960-1686(93)90275-4.
- Ruben, S. M., D. M. Mannini, F. C. Holschuh, T. C. Holshuh, M. D. Wilson, and T. Holschuh, 1995: Emergency room visits for asthma and chronic obstructive pulmonary disease on the Island of Hawai'i, 1981–1991. *Proc. Earthquake, Tsunami, and Volcano Hazards Seminar*, Hilo, HI, University of Hawaii at Hilo.
- Ryaboshapko, A., and Coauthors, 2007: Intercomparison study of atmospheric mercury models: 2. Modelling results vs. long-term observations and comparison of country deposition budgets. *Sci. Total Environ.*, **377**, 319–333, doi:10.1016/j.scitotenv.2007.01.071.
- Schiferl, L. D., and Coauthors, 2014: An investigation of ammonia and inorganic particulate matter in

- California during the CalNex campaign. *J. Geophys. Res. Atmos.*, **119**, 1883–1902, doi:10.1002/2013JD020765.
- Schroeder, T. A., 1981: Characteristics of local winds in northwest Hawaii. *J. Appl. Meteor.*, **20**, 874–881, doi:10.1175/1520-0450(1981)020<0874:COLWIN>2.0.CO;2.
- Skamarock, W. C., J. B. Klemp, J. Dudhia, D. O. Gill, D. M. Barker, W. Wang, and J. G. Powers, 2005: A description of the advanced research WRF version 2. NCAR Tech. Note NCAR/TN-468+STR, 88 pp. [Available online at www.mmm.ucar.edu/wrf/users/docs/arw_v2.pdf.]
- Sutton, A. J., and T. Elias, 1993: Volcanic gases create air pollution on the island of Hawai'i. *Earthquakes and Volcanoes*, Vol. 24, U.S. Geological Survey, Reston, VA, 178–196.
- , and —, 1997: Volcanic gases, vog and laze: What they are, where they come from, and what they do. *Proc. Vog and Laze Seminar*, Hilo, HI, Federal Emergency Management Agency, 1 pp. [Available online at <http://hvo.wr.usgs.gov/products/1997pub.html>.]
- , —, J. W. Hendley II, and P. H. Stauffer, 1997: Volcanic air pollution—A hazard in Hawaii: USGS Fact Sheet 169-97, 2 pp.
- , —, T. M. Gerlach, and J. B. Stokes, 2001: Implications for eruptive processes as indicated by sulfur dioxide emissions from Kilauea Volcano, Hawai'i, 1979–1997. *J. Volcanol. Geotherm. Res.*, **108**, 283–302, doi:10.1016/S0377-0273(00)00291-2.
- Tam, E. K., and Coauthors, 2007: Volcanic air pollution and respiratory symptoms in schoolchildren on the Big Island of Hawai'i. *Proc. ATS 2007*, San Francisco, CA, American Thoracic Society, A168.
- Williams-Jones, G., K. A. Horton, T. Elias, H. Garbeil, P. Mougini-Mark, A. J. Sutton, and A. J. L. Harris, 2006: Accurately measuring volcanic plume speeds with multiple UV spectrometers. *Bull. Volcanol.*, **68**, 328–332, doi:10.1007/s00445-005-0013-x.
- Wilson, D., T. Elias, T. Orr, M. Patrick, J. Sutton, and D. Swanson, 2008: Small explosion from new vent at Kilauea's summit. *Eos, Trans. Amer. Geophys. Union*, **89**, 203, doi:10.1029/2008EO220003.
- Worth, R. M., 1995: Respiratory impacts associated with chronic VOG exposure on the Island of Hawai'i. *Proc. Vog and Laze Seminar*, Honolulu HI., Hawaii State Department of Health.

NEW FROM AMS BOOKS!

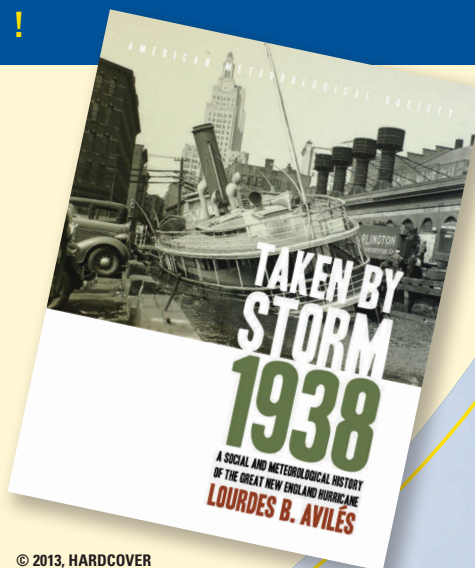
“An engrossing account of New England’s worst natural catastrophe.”

— KERRY EMANUEL, *Professor of Atmospheric Science, MIT*

Taken by Storm, 1938: *A Social and Meteorological History of the Great New England Hurricane*

LOURDES B. AVILÉS

When the Great New England Hurricane of 1938 hit the Northeast unannounced, it changed everything from the landscape, to Red Cross and Weather Bureau protocols, to the measure of Great Depression relief New Englanders would receive, and the resulting pace of regional economic recovery. The science behind this storm is presented here for the first time, with new data that sheds light on the motivations of the Weather Bureau forecasters. This compelling history successfully weaves science, historical accounts, and social analyses to create a comprehensive picture of the most powerful and devastating hurricane to hit New England to date.



© 2013, HARDCOVER
ISBN: 978-1-878220-37-0
LIST \$40 MEMBER \$30

AMS BOOKS

RESEARCH APPLICATIONS HISTORY

www.ametsoc.org/amsbookstore